

S-HR-VQVAE: Sequential Hierarchical Residual Learning Vector Quantized Variational Autoencoder for Video Prediction

Mohammad Adiban[†], Kalin Stefanov^{*}, Sabato Marco Siniscalchi[†], Giampiero Salvi^{†¶}

[†]Norwegian University of Science and Technology, Faculty of Information Technology and Electrical Engineering

[¶]KTH Royal Institute of Technology, School of Electrical Engineering and Computer Science

^{*}Monash University, Faculty of Information Technology

E-mails: {mohammad.adiban,marco.siniscalchi,giampiero.salvi}@ntnu.no, kalin.stefanov@monash.edu



Abstract—We address the video prediction task by putting forth a novel model that combines (i) our recently proposed hierarchical residual vector quantized variational autoencoder (HR-VQVAE), and (ii) a novel spatiotemporal PixelCNN (ST-PixelCNN). We refer to this approach as a sequential hierarchical residual learning vector quantized variational autoencoder (S-HR-VQVAE). By leveraging the intrinsic capabilities of HR-VQVAE at modeling still images with a parsimonious representation, combined with the ST-PixelCNN’s ability at handling spatiotemporal information, S-HR-VQVAE can better deal with chief challenges in video prediction. These include learning spatiotemporal information, handling high dimensional data, combating blurry prediction, and implicit modeling of physical characteristics. Extensive experimental results on the KTH Human Action and Moving-MNIST tasks demonstrate that our model compares favorably against top video prediction techniques both in quantitative and qualitative evaluations despite a much smaller model size. Finally, we boost S-HR-VQVAE by proposing a novel training method to jointly estimate the HR-VQVAE and ST-PixelCNN parameters.

Index Terms—Video Prediction, Hierarchical Modeling, Autoregressive Modeling

1 INTRODUCTION

Sequence learning focuses on the development of algorithms for the analysis of sequential data found in a wide variety of domains including, computer vision, natural language processing, speech processing, and bioinformatics [1], [2]. Sequence learning algorithms typically operate on input sequences that consist of a series of discrete or continuous observations, such as letters, words, video frames, and audio samples. The goal of sequence learning algorithms is to learn patterns and relationships within the sequential data that can be used to make predictions about future unseen data.¹ This may involve modeling the probability distribution of the sequential data, identifying common

subsequences or motifs, and learning to predict the next observation in the sequence. Sequence learning for *video prediction* refers to future video frame anticipation given a set of preceding frames [3]. This is a challenging task because it requires the algorithm to learn complex spatiotemporal relationships within the video.

The video prediction task poses four main challenges related to (i) spatiotemporal modeling, (ii) high dimensionality, (iii) blurry predictions, and (iv) physical characteristics. The spatiotemporal modeling challenge is concerned with capturing spatiotemporal dependencies in sequences of video frames, which is related to humans’ ability to understand their surrounding physical world and is related to accurate modeling of videos [4]. High dimensionality is intrinsic to video patterns, and high-dimensional patterns pose the problem referred to as the curse of dimensionality in function approximation and optimization [5]. Blurry predictions are caused by the properties of many statistical models that tend to produce fuzzier outputs when predicting future events that are inherently affected by higher uncertainty. The challenge of physical characteristics refers to the properties and attributes of the objects (e.g., shape, size, color) and scenes (e.g., lighting conditions) captured in a video that may affect the prediction task. If modeled properly, those characteristics may be easier to predict in future frames.

This paper proposes a sequential hierarchical residual learning vector quantized variational autoencoder (S-HR-VQVAE) for the task of video prediction with the goal of addressing the abovementioned challenges. In particular, S-HR-VQVAE implements major extensions to two non-time sequential algorithms: 1) Our recent work on hierarchical residual learning vector quantized variational autoencoder for image reconstruction and generation, HR-VQVAE [6] and 2) An autoregressive generative model that captures the distribution of dependencies between image pixels, PixelCNN [7], [8]. In particular, the proposed S-HR-VQVAE

1. This work has been submitted to the IEEE for possible publication. Copyright may be transferred without notice, after which this version may no longer be accessible.

technique consists of three steps. In the first step, the input video frames are encoded to a continuous latent space and then mapped to discrete representations through the hierarchical vector quantization encoder of HR-VQVAE, with each latent vector assigned to a codeword in a codebook. The key property of this model is the strict hierarchy imposed between codebooks belonging to different layers in the model, producing extremely compact and efficient discrete representations. In the second step, in order to predict the latent representations of future frames, we propose a spatiotemporal PixelCNN (ST-PixelCNN) where the distribution of the discrete representation for a particular location in the current frame is conditioned on the representations for neighboring locations both in space and time. In the third step, the predicted discrete representation is used by the decoder of HR-VQVAE to generate the corresponding video frame.

Our contributions can be summarized as follows.

- A novel model is proposed to address the video prediction task, namely S-HR-VQVAE, that has the property of capturing different levels of abstraction in a sequence of video frames. Higher layers capture the context; whereas lower layers focus on the details. This model is a significant extension of previously proposed methods such as HR-VQVAE and PixelCNN, as will be detailed in the method section. Leveraging hierarchical VQ within the VAE framework [9], S-HR-VQVAE is able to better contrast the blurring phenomenon encountered in video prediction, e.g., [4], while better handling the high-dimensionality issue. Furthermore, by combining HR-VQVAE properties discussed in [6] with the newly introduced ST-PixelCNN, S-HR-VQVAE well captures spatiotemporal dependencies and physical characteristics. Finally, S-HR-VQVAE also owns the property of significantly reducing the time required for training and inference.
- A thorough and systematic experimental validation of the contributions of S-HR-VQVAE is presented while providing an extensive account and comparison with state-of-the-art in video prediction techniques over two video sequence prediction tasks, namely the Moving-MNIST task [10], and the KTH Human Action task [11].
- A novel loss function to jointly train the HR-VQVAE and the ST-PixelCNN is introduced, which is experimentally proven to boost S-HR-VQVAE over the Moving-MNIST, and KTH Human Action tasks, and across several metrics.

The rest of the paper is organized as follows. Section 2 presents the related works, grouped accordingly to the four aforementioned challenges. Section 3 gives the key concepts necessary to introduce our technique. The proposed method is described in Section 4. The experimental setup and related results are discussed in Sections 5, and 6, respectively. Section 7 discusses some key properties of the proposed technique. Section 8 concludes the present work.

2 RELATED WORK

2.1 Spatiotemporal Modeling

Several studies focused on extracting spatial information from videos. Hu et al. [12] proposed DrNet to model spatial features in single video frames, but temporal information was not taken into account. McNet [13] was proposed to model the motion (temporal) and content (spatial) aspects, which were however treated as independent sources of information. MsNet [14] introduced mutual suppression adversarial training to acquire disentangled motion and content representations. Both McNet and MsNet neglect possible joint correlations between spatial and temporal aspects in video frames. In [15], ConvLSTM was thus introduced to capture joint spatial and temporal correlations in video frames, where visual representations are extracted by exploiting convolutions in both input-to-state and state-to-state transitions. Unfortunately, ConvLSTM has a few shortcomings, including difficulty in capturing long-term dependencies, limited ability to model complex temporal patterns and poor scalability.

To address ConvLSTM deficiencies, Wang et al. [16] proposed a new architecture based on spatiotemporal LSTM, referred to as PredRNN, employing (i) complex nonlinear transition functions from one frame to the next, and (ii) a dual memory structure. Unfortunately, PredRNN struggles to model complex long-term dependencies in the data, which can result in poor future frames prediction. PredRNN++ [17] was therefore devised to address some of PredRNN’s limitations, introducing a different hierarchical recurrent structure that captures dependencies at multiple timescales. PredRNN-V2 [18] was also proposed to improve PredRNN by traversing all nodes of PredRNN in a zigzag path of bi-directional hierarchies in order to jointly model spatial correlations and temporal dynamics. Motivated by PredRNN and PredRNN++, Wang et al. [19] put forth E3D-LSTM, the eidetic 3D memory cell with a short-time convolution window with spatiotemporal connection chain of convolutional LSTM blocks.

Su et al. [20] improved the efficiency of higher-order ConvLSTMs by leveraging low-rank tensor factorization. This model effectively captured both visual appearances and temporal dynamics leveraging new recurrent mechanism, such as “spatiotemporal memory flow,” and new training procedures. In [21], a novel model, dubbed Robust-ST-ConvLSTM (R-ST-LSTM), was introduced to extend ConvLSTM leveraging a novel spatiotemporal unit based on memory flow. R-ST-LSTM demonstrated a remarkable performance improvement in long-term frame prediction tasks. Nevertheless, a constraint of these approaches lies in their ability to encode long-term dynamics since it predominantly relies on the input sequence to establish relationships between frames. As a result, capturing the comprehensive long-term motion context for accurate future prediction becomes challenging, particularly when the input sequence exhibits limited dynamics.

To address the spatiotemporal challenge, we propose ST-PixelCNN: First, we extend PixelCNN with causal convolutions in time and spatiotemporal self-attention to model the spatiotemporal correlations. Then, we make the model

operate on the latent discrete representations produced by HR-VQVAE rather than on the pixels directly.

2.2 High Dimensionality

The aforementioned spatiotemporal methods rely on exceedingly complex modeling, which limits their scalability, especially with the high dimensionality of video data. To overcome this issue, Hsieh et al. [22] tried to capture spatiotemporal information by dividing frames into patches and predicting their evolution in the time given previous neighboring patches. Then, a recurrent convolutional neural network (rCNN) [23] is employed to generate the next frame. Jun-Ting et al. [24] proposed the decompositional disentangled predictive autoencoder (DDPAE) framework, which is a combination of a structured probabilistic model, and deep neural networks. The framework automatically decomposes the high-dimensional video into components and disentangles each component to have low-dimensional temporal dynamics. A probabilistic motion sampling model is described by Xue et al. [25] based on variational autoencoder (VAE) [9], in which a generative encoder-decoder network is trained to generate a distribution of the next frame predictions. Oliu et al. [26] proposed the folded recurrent neural network (fRNN), a recurrent autoencoder architecture featuring a gated recurrent unit (GRU) that implements a bi-directional flow of the information, by enabling state sharing between the encoder and decoder. Razali and Fernando devised V-3D-ConvLSTM [27], which relies on variational encoder-decoder and 3D-ConvLSTM to benefit from both techniques. Ye and Bilodeau [28] developed an attention mechanism based encoder-decoder, called VPTR, to learn local spatiotemporal representation while reducing the complexity of standard transformer models.

S-HR-VQVAE can effectively manage the high dimensionality of video data utilizing HR-VQVAE that efficiently compresses each video frame because of its strict hierarchical nature.

2.3 Blurry Predictions

The use of RNNs, VAEs, and their variants, such as variational RNNs (VRNNs) [29], is widespread in video prediction. However, these approaches frequently result in blurry predictions, as reported in various studies [30], [31]. This issue is typically attributed to the use of a similarity metric in the pixel space [30], [32], such as mean squared error (MSE), which corresponds to a log-likelihood loss under a fully factorized Gaussian distribution. Such models and loss functions are unable to accommodate the inherent uncertainty of future events, leading to blurry predictions on average. Two main strategies have emerged to address this issue: 1) Latent variable methods that explicitly model underlying stochasticity, and 2) Adversarially-trained models that aim to produce more natural images.

Babaeizadeh et al. [33] and Denton and Fergus [34] aimed to investigate stochastic models for video prediction using the VAE framework. Given the recent advances in generative adversarial networks (GANs), researchers have explored alternative generative models such as VAE-GANs [30], [31] for video frame prediction. In those models, VAE was adopted to model dynamic frame transitions by

latent variables. Then, the GAN was fed with the latent variables combined with previous frames as an extra input to improve the diversity of the model and increase the precision of the next frame prediction. VAE-GANs allow capturing stochastic posterior distributions of videos while making it feasible to model the spatiotemporal joint distribution of pixels. However, such methods often suffer from the problem of mode collapse and unrealistic predictions [31], [33].

S-HR-VQVAE utilizes HR-VQVAE which is effective in high-quality image reconstruction and generation while minimizing the image blur. This is achieved through its hierarchical codebooks which can efficiently benefit from increasing the depth of the hierarchy. Although the compressed encoding is lossy, the original video can still be reconstructed with a high degree of fidelity through the latent representations, which is demonstrated by our thorough experiments.

2.4 Physical Characteristics

Most of the discussed methods represent the information contained in the videos as a whole. However, videos are usually made of slowly varying contextual information, such as the background [35] and a number of objects in the foreground that possibly vary more quickly following specific physical rules [36]. For example, object velocity tends to be constant, and deformation in the human body can be modeled by joints and rods.

In order to benefit from those physical characteristics, some approaches proposed pixel-level representations. For instance, De Brabandere et al. [37] developed a dynamic filter network (DFN) to learn local spatial transformations by picking up flow information. Finn et al. [38] proposed the convolutional dynamic neural advection (CDNA), an action-conditioned predictive model that tries to learn physical object motion and predict the distribution over pixel motion from previous frames. Liu et al. [39] proposed a system that learns to predict optical flows between future and past frames. Berg et al. [40] employed backward content transformation to learn the future to the past through a 6-parameter affine model.

The dense motion field can also be represented in the form of a pixel-adaptive convolutional kernel convolved with past frames to synthesize future frames. To capture the motion and content features independently, Villegas et al. [13] took advantage of LSTM and modeled the images at the pixel level to capture the spatial layout. The temporal dynamics were independently modeled again using an LSTM to simplify the prediction task. Lee et al. [41] proposed LMC-memory model to predict future frames considering the long-term motion context. Although LMC-memory tries to deal with the high dimensionality of videos, most of the methods in this section are limited to physical characteristics while other video prediction challenges such as high dimensionality, blurry predictions, and spatiotemporal modeling were underestimated or overlooked.

Although S-HR-VQVAE does not explicitly model physical characteristics, it leverages the modularity of the HR-VQVAE to implicitly model those. More specifically, this is accomplished by decomposing the latent representations

into a hierarchy of discrete codes and separating high-level, global information from details (such as fine texture or small motions). Since the latent representations are decomposed into different layers of hierarchical residual codes, the proposed ST-PixelCNN can exploit spatiotemporal dependencies that are different for different levels of details. For example, the background evolves slowly in time; whereas, the foreground object may move quicker. Similarly, within the foreground object, some details, such as hands and arms, may exhibit different movement patterns compared to the body. The combination of HR-VQVAE and ST-PixelCNN allows us to model those phenomena in a very efficient way improving accuracy at the same time as reducing complexity.

3 THEORETICAL BACKGROUND

In this section, we provide the background and introduce the key concepts that are necessary to understand the proposed method, which is discussed in Section 4.

3.1 VQVAE

Variational autoencoders (VAEs) are probabilistic models that aim to reconstruct the input data from a lower-dimensional representation obtained with a bottleneck layer in the model. An extension of VAEs is vector quantized variational autoencoders (VQVAEs), where the latent representation is discretized. In specific problems, these models may result in good reconstruction with even lower dimensional discrete representations than VAEs. Furthermore, the discrete representation may be easier to interpret compared to the bottleneck features in VAEs. VAEs and VQVAEs have been used for many applications. In the following treatment, we will focus on images, as these are most relevant to our work. An input image is a tensor $\mathbf{x} \in \mathbb{R}^{H_I \times W_I \times D_I}$ of height H_I , width W_I and D_I color channels. VQVAEs first map the input image \mathbf{x} to a continuous latent vector $\mathbf{z} \in \mathbb{R}^{H \times W \times D}$ through a non-linear encoder: $\mathbf{z} = E(\mathbf{x})$. Next, each element $\mathbf{z}_{hw} \in \mathbb{R}^D$, with $h \in [1, H]$, and $w \in [1, W]$, in the continuous latent vector \mathbf{z} is quantized to the nearest codebook vector (i.e., a codeword) $\mathbf{e}_k \in \mathbb{R}^D$, $k \in 1, \dots, m$ by

$$\text{Quantize}(\mathbf{z}_{hw}) := \mathbf{e}_k \text{ where } k = \arg \min_j \|\mathbf{z}_{hw} - \mathbf{e}_j\|_2. \quad (1)$$

The quantized vectors corresponding to each element \mathbf{z}_{hw} are then recombined into the quantized continuous representation $\mathbf{e} \in \mathbb{R}^{H \times W \times D}$ to form the input of the decoder that reconstructs the input image using a non-linear transformation $\mathcal{D}(\cdot)$. The loss function $\mathcal{L}(\cdot)$ aims at minimizing the reconstruction error $\|\mathbf{x} - \mathcal{D}(\mathbf{e})\|_2$ whilst minimizing the quantization error $\|\mathbf{z} - \mathbf{e}\|_2$ as follows

$$\mathcal{L}(\mathbf{x}, \mathcal{D}(\mathbf{e})) = \|\mathbf{x} - \mathcal{D}(\mathbf{e})\|_2^2 + \|\text{sg}[\mathbf{z}] - \mathbf{e}\|_2^2 + \beta \|\text{sg}[\mathbf{e}] - \mathbf{z}\|_2^2, \quad (2)$$

where $\text{sg}(\cdot)$ is a stop-gradient operator that cuts the gradient flow through its argument during the backpropagation, and β refers to a hyperparameter that controls the reluctance to change the latent vectors corresponding to the encoder output.

VQVAE-2 [42] is a multi-layer version of the VQVAE that compresses images into several latent vectors, from the *top* layer (smaller size) to the *bottom* layer (larger size). The

bottom layer is conditioned on the top layer so that the top layer extracts general information from the image; whereas, the bottom layer focuses on details to reconstruct the input image. The codebooks at different layers, however, are not related by a hierarchy.

3.2 HR-VQVAE

In [6], we proposed a truly hierarchical version of VQVAE, dubbed HR-VQVAE, and that is one of the building blocks of the video prediction method proposed in this work. HR-VQVAE deals with limitations in techniques such as VQVAE and VQVAE-2, e.g., codebook collapse and non-locality in codewords' indices [6]. In HR-VQVAE, each layer captures residual information that is not properly modeled by the preceding layers. Differently from VQVAE-2, in HR-VQVAE the codebooks at different layers are constrained by a strict hierarchy. The aspects of HR-VQVAE that are relevant to the proposed method will be detailed in Section 4. Further details on this method can be found in [6].

4 PROPOSED METHOD

The overall framework of the proposed approach is depicted in Fig. 1. Given T input frames $(\mathbf{x}_1, \dots, \mathbf{x}_T)$ in a video, the goal is to predict the following S frames $(\mathbf{x}_{T+1}, \dots, \mathbf{x}_{T+S})$. The approach follows three steps. First, the input frames are encoded into a discrete latent representation using HR-VQVAE. In the second step, we propose a method, we call spatiotemporal PixelCNN (ST-PixelCNN), to predict new discrete latent variables of future frames based on the latent variables for previous frames. In the final step, the HR-VQVAE decoder is used to generate the new frames from the latent variables obtained by ST-PixelCNN. In the following, we will detail each of the above steps and describe two methods for training HR-VQVAE and ST-PixelCNN either independently or jointly. We refer to the whole model as sequential hierarchical residual learning vector quantized variational autoencoder (S-HR-VQVAE).

4.1 Step 1: Frame Encoding

In this step, each frame $\mathbf{x} \in \mathbb{R}^{H_I \times W_I \times D_I}$ is encoded using HR-VQVAE into a discrete latent representation. HR-VQVAE first encodes the frame into a continuous vector $\mathbf{z} = E(\mathbf{x}) \in \mathbb{R}^{H \times W \times D}$. These vectors are then iteratively quantized into n hierarchical layers of discrete latent embeddings. Assuming the first layer has a codebook of size M , the second layer has M independent codebooks of size M (for a total of M^2 codewords), and so on. A generic layer i has M^{i-1} codebooks of size M , for a total of M^i codewords. However, only one of those codebooks is used in each layer depending on which codewords were chosen in the previous layers. In each layer i , the codebook is optimized to minimize the error between the codewords $\mathbf{e}_k^i \in \mathbb{R}^D$ and the elements $\xi_{hw}^{i-1} \in \mathbb{R}^D$ of the residual error from the previous layer²

$$\text{Quantize}^i(\xi_{hw}^{i-1}) := \mathbf{e}_k^i \text{ where } k = \arg \min_j \|\xi_{hw}^{i-1} - \mathbf{e}_j^i\|_2, \quad (3)$$

2. For the first layer, $\xi_{hw}^0 \equiv \mathbf{z}_{hw}$.

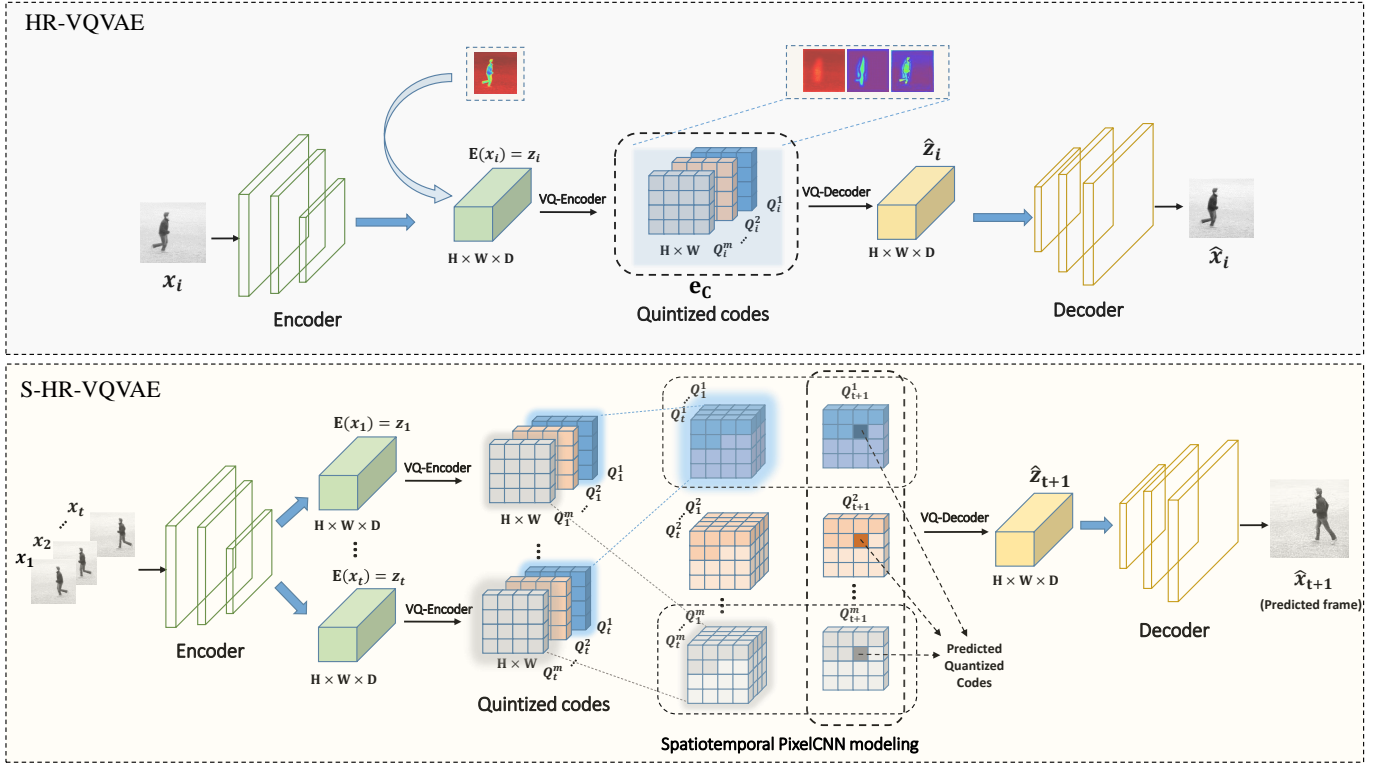


Fig. 1: The architecture of the proposed approach. Top: HR-VQVAE for static image reconstruction. Bottom: S-HR-VQVAE for video prediction.

and e_k^i belongs to one of the possible codebooks $C_i(t)$ for layer i . Which codebook is used is determined by the codeword e_t^{i-1} selected at the previous layer. Within each layer, the codewords e_k^i , for each element ξ_{hw}^{i-1} of the residual, are combined to form the tensor $e^i \in \mathbb{R}^{H \times W \times D}$. Across the different layers, the tensors e^i are then summed to form the “combined” discrete representation e_C . When HR-VQVAE is used to reconstruct single images, e_C is fed into the decoder to reconstruct the image as $\hat{x} = \mathcal{D}(e_C)$, and the corresponding objective function is used to train the system

$$\begin{aligned} \mathcal{L}(x, \mathcal{D}(e_C)) &= \|x - \mathcal{D}(e_C)\|_2^2 + \|\text{sg}[\xi^0] - e_C\|_2^2 \\ &+ \beta_0 \|\text{sg}[e_C] - \xi^0\|_2^2 + \sum_{i=1}^n \mathcal{L}(\xi^{i-1}, e^i), \end{aligned} \quad (4)$$

with

$$\mathcal{L}(\xi^{i-1}, e^i) = \|\text{sg}[\xi^{i-1}] - e^i\|_2^2 + \beta_i \|\text{sg}[e^i] - \xi^{i-1}\|_2^2. \quad (5)$$

The β_i are hyperparameters that control the reluctance to change the code corresponding to the encoder output. The main goal of Eqs. 4, and 5 is to make a hierarchical mapping of input data in which each layer of quantization extracts residual information from its bottom layers.

In S-HR-VQVAE, the method proposed in this work, however, we do not reconstruct images directly. Instead, the indices to the codewords e^i are used as latent representations for each input frame in the video and each layer in the system and are input to the video prediction steps described below. We call these indices for layer i , $Q^i \in [1, M]^{H \times W}$, with M the size of each codebook.

4.2 Step 2: Spatiotemporal Latent Representation Prediction

The next step in the proposed method uses the indices (Q_1^i, \dots, Q_T^i) of the codewords (e_1^i, \dots, e_T^i) obtained from each layer i of HR-VQVAE from the input frames (x_1, \dots, x_T) , to predict the indices $(Q_{T+1}^i, \dots, Q_{T+S}^i)$ of the codewords $(e_{T+1}^i, \dots, e_{T+S}^i)$ for S future frames, with the goal of later predicting the S future frames $(x_{T+1}, \dots, x_{T+S})$ in the final step.

For this task, we propose an extension to PixelCNN (see Figure. 1-b). The original PixelCNN uses a spatial autoregressive model on pixels. The proposed spatiotemporal PixelCNN (ST-PixelCNN) extends the autoregressive model of the original PixelCNN in time. This allows the model to predict the future codeword indices $\hat{Q}_{t>T}$ using the codeword indices at previous times (Q_1^i, \dots, Q_T^i) . Furthermore, the original PixelCNN operated directly on the pixel values. Our method takes as input discrete indices of the latent representations and predicts future indices. Combined with the hierarchical nature of HR-VQVAE, this simplifies considerably the spatial and temporal prediction problem, allowing our model to focus on the essential aspects of the frames that vary in space and time.

In order to explain the proposed extended probabilistic model, we first order the elements of $Q_t^i \in [1, M]^{H \times W}$, from left to right and from top to bottom using a linear index $v_k \in [1, HW]$. Then we use the notation $v_{j < k}$ to refer to any element of Q_t^i to the left or the top of v_k . Given the above

TABLE 1: Configuration details for the S-HR-VQVAE architecture.

| | KTH Human Action | | | Moving-MNIST | | |
|-----------------------------|------------------|--------------|------------------|--------------|-------------|-----------------|
| | | | | | | |
| Input size | 128 × 128 × 3 | | | 64 × 64 × 1 | | |
| Bit rate | 8 | | | 8 | | |
| Latent size | 32 × 32 × 8 | | | 16 × 16 × 4 | | |
| Quantized latent size | 32 × 32 | | | 16 × 16 | | |
| Num. of hierarchy layers | 1 | 3 | 9 | 1 | 3 | 6 |
| Codebook size | 512 | 8 | 2 | 64 | 4 | 2 |
| Num. of codewords in layers | 512 | {8, 64, 512} | {2, 4, ..., 512} | 64 | {4, 16, 64} | {2, 4, ..., 64} |
| Compression ratio | ≈42.66 | ≈42.66 | ≈42.66 | ≈21.33 | ≈21.33 | ≈21.33 |

notation, the extended probabilistic model can be written as

$$p(\hat{Q}_{t+1}^i(v_k)) = \prod_{j=1}^{H \times W} p(\hat{Q}_{t+1}^i(v_{j < k}) | Q_1^i(v_{j < k}), \dots, Q_t^i(v_{j < k})), \quad (6)$$

where \hat{Q}_t^i represents the predicted quantized discrete codes of layer i obtained from the t^{th} frame.

The above behavior is obtained by using convolutional masks to limit the information that is used during prediction. The convolutional masks were applied in a manner consistent with the original PixelCNN, constraining the convolutions to retrieve only spatial information from the left and above each pixel. For the temporal dimension, convolutions were restricted to previous time steps by masking out present and future timesteps. This strategy is implemented using multi-head attention layers analogous to [42]. However, here the attention is applied to 3D voxels.

The loss function of ST-PixelCNN is as follows

$$\begin{aligned} \mathcal{L}_p(p(Q_{t>T}^i), p(\hat{Q}_{t>T}^i)) = & \\ - \frac{1}{H \times W} \sum_{j=1}^{H \times W} \sum_{m=1}^M p(Q_{t>T}^i[j, m]) * \log p(\hat{Q}_{t>T}^i[j, m]), & \end{aligned} \quad (7)$$

4.3 Step 3: Frame Generation

Once the quantization indices \hat{Q}_t^i for each layer i and each time step $t \in [T+1, T+S]$ have been estimated by the ST-PixelCNN, the corresponding quantized representation $\hat{\mathbf{z}}_t \in \mathbb{R}^{H \times W \times D}$ can be easily computed by codebook access in a similar manner as done for \mathbf{e}_C in the original HR-VQVAE (see Section 4.1).

$$(\hat{\mathbf{x}}_{T+1}, \dots, \hat{\mathbf{x}}_{T+S}) = (\mathcal{D}(\hat{\mathbf{z}}_{T+1}), \dots, \mathcal{D}(\hat{\mathbf{z}}_{T+S})), \quad (8)$$

where the $\hat{\mathbf{z}}_{t>T}$ and $\hat{\mathbf{x}}_{t>T}$ represent the predicted latent representations and frames, respectively.

4.4 Disjoint and Joint Training

HR-VQVAE and ST-PixelCNN in the combined model described above can be trained independently. In this case, we first train HR-VQVAE according to Eq. 4 to predict each frame \mathbf{x}_i in the video independently of the others. By doing this, we obtain a sequence of latent representations $(Q_1^i, \dots, Q_T^i, Q_{T+1}^i, \dots, Q_{T+S}^i)$ for each layer in HR-VQVAE and for the complete sequence of frames. We can now train the ST-PixelCNN to predict the sequence $(Q_{T+1}^i, \dots, Q_{T+S}^i)$ given the input sequence (Q_1^i, \dots, Q_T^i) ,

by optimizing Eq. 7. In the test phase, we use the predictions of ST-PixelCNN in combination with the HR-VQVAE decoder to predict unseen video frames, making sure that the combined model only has access to $(\mathbf{x}_1, \dots, \mathbf{x}_T)$ when predicting $(\mathbf{x}_{T+1}, \dots, \mathbf{x}_{T+S})$.

Following this training procedure, the decoder in HR-VQVAE is exclusively optimized to deal with the uncertainty introduced by the encoder of HR-VQVAE. When reconstructing the frames $(\mathbf{x}_{T+1}, \dots, \mathbf{x}_{T+S})$, however, we also need to deal with the uncertainty introduced by the ST-PixelCNN predictions.

In an attempt to address this issue, we introduce an alternative training approach that optimizes ST-PixelCNN and the HR-VQVAE decoder jointly. The joint training is guided by two distinct objectives: the loss for the HR-VQVAE decoder, represented by the first term of Eq. 4, and the ST-PixelCNN loss in Eq. 7. The corresponding multi-objective loss is

$$\mathcal{L}_{\text{joint}} = \mathcal{L}_p + \lambda \|\mathbf{x} - \mathcal{D}(\mathbf{e}_C)\|_2^2, \quad (9)$$

where λ is a hyperparameter that controls the effect of the reconstruction loss on the joint training. In this case, during training, HR-VQVAE only produces the latent representations (Q_1^i, \dots, Q_T^i) for the input frames $(\mathbf{x}_1, \dots, \mathbf{x}_T)$. The latent representations $(Q_{T+1}^i, \dots, Q_{T+S}^i)$ for the frames $(\mathbf{x}_{T+1}, \dots, \mathbf{x}_{T+S})$ are predicted by ST-PixelCNN and then used to train the HR-VQVAE decoder.

5 EXPERIMENTS

In this section, we first introduce the datasets used in the conducted experiments, followed by the overall experimental setup. In our experiments, we adopted common metrics for the quantitative analysis to assess the proposed solution, and those metrics are also detailed in this section.

5.1 Datasets

The **Moving-MNIST** dataset is a variant of the MNIST handwritten digits dataset [10]. Each sequence in the dataset spans 20 consecutive frames displaying two digits moving within a 64×64 frame. The digits move with a constant velocity and pre-defined angle. The dataset has a fixed number of entries, with 10,000 sequences for training and 5,000 sequences for testing.

The **KTH Human Action** dataset [11] is a moving image dataset with a resolution of 160x120 pixels that contains six

types of human actions, including walking, jogging, running, boxing, hand waving, and hand clapping. The dataset comprises 25 human subjects performing actions in four different scenarios. For our experiments, we followed [18], resized the video frames down to 128×128 , and split the dataset into two subsets: (i) a training set, consisting of the first 16 subjects’ actions, and (ii) a test set, containing the remaining subjects (subjects 17-25). The training set consists of 108,717 sequences; whereas, the test set includes 4,086 sequences.

5.2 Experimental Setup

Table 1 lists some details about S-HR-VQVAE architecture for tackling the Moving-MNIST and the KTH Human Action tasks. *Input size* refers to the initial resolution of the video frames. *Latent size* corresponds to the continuous latent representation in HR-VQVAE. *Quantized latent size* to the quantized representation in the model. Table 1 also specifies additional information including the bit rate, number of hierarchy layers, codebook size, number of codewords, and compression ratio.

The proposed S-HR-VQVAE was trained on sequences consisting of 10 consecutive frames with the goal of predicting 10 future frames for Moving-MNIST, and 20 future frames for KTH Human Action, which is a common practice for the two tasks. In all experiments, the neural model is trained using the Adam optimizer [43], and the learning rate is set to 0.0003 for both HR-VQVAE encoder-decoder and ST-PixelCNN. Besides, λ in Eq. 9 is set to 0.11.

5.3 Metrics

We report results adopting metrics that are commonly used in the literature, namely: peak signal-to-noise ratio (PSNR) [44], structural similarity index measure (SSIM) [45], learned perceptual image patch similarity (LPIPS) [46], and mean square error (MSE).

PSNR, SSIM, MSE, and LPIPS are all image quality metrics but differ in their characteristics. PSNR focuses on signal-to-noise ratio, SSIM considers structural similarity, MSE measures pixel-wise differences, and LPIPS aims to capture perceptual similarity based on deep neural networks. All those metrics, however, have limitations. For example, PSNR and MSE have been shown to have poor correlation with human perception [47], [48] and may not take into account higher-level semantic information, such as in action modeling. SSIM and LPIPS are more effective in capturing perceptual differences, but they may not be as effective at capturing differences in color or texture as at capturing differences in luminance and contrast [49]. Therefore, it is important to take into account several metrics to better capture different aspects of the video prediction task and obtain a more comprehensive assessment of the method’s performance. In our experiments, we report results according to all those metrics and include all available results for the related methods.

Because of the limitations of these metrics, we also report a qualitative assessment to verify whether the metrics have missed some important aspects of the video prediction task.

6 RESULTS

In this section, we present the results of the quantitative evaluation of the proposed method, followed by a qualitative assessment. In order to better appreciate the effectiveness of the proposed technique, we have performed a systematic review of reported quantitative results of recent, state-of-the-art solutions on the two selected tasks, namely Moving-MNIST, and KTH Human Action.

The qualitative analysis is performed by observing the behavior of the proposed method on several video sequences, which is a common practice in the research field. However, while reviewing the literature, we noticed that different methods use different video sequences to visually demonstrate the quality of their approaches; furthermore, the source code is not available for all methods in the literature, which implies that different systems can not be compared on the same set of predefined video sequences. To overcome that issue, we first selected video sequences common among different techniques in the literature. Then, we evaluated our S-HR-VQVAE on those selected examples and grouped the results accordingly. To the best of our knowledge, this is the first time that such a systematic comparison has been carried out for the Moving-MNIST, and the KTH Human Action datasets.

Finally, we also investigated other features of the proposed S-HR-VQVAE method, namely: (i) compression and reconstruction capabilities, (ii) blur mitigation, and (iii) noise removal effectiveness.

6.1 Quantitative Analysis

In this study, we assess the performance of state-of-the-art video prediction methods on the KTH Human Action and Moving-MNIST datasets, providing a comprehensive overview of the advancements in the field. In particular, Table 2 lists state-of-the-art methods from 2015 to 2023 in a chronologically ascending order, highlighting thereby the evolution of the techniques over the years. S-HR-VQVAE results are reported in the last two rows with disjoint and joint training, respectively. On the KTH Human Action task, PSNR and SSIM are reported by all state-of-the-art techniques; whereas LPIPS is provided for only a few methods. On the Moving-MNIST task, SSIM and MSE are reported by most of the state-of-the-art techniques; whereas PSNR is provided by only a few of them.

Referring to Table 2, we can observe that the different metrics improve over the years. However, when trying to determine the best method, we observe that methods performing best in one metric are usually outperformed by other methods in other metrics. For example, for KTH Human Action, R-ST-ConvLSTM [21] attains the best PSNR but not the best SSIM which was obtained by Conv-TT-LSTM [20]. Similarly for LPIPS, PredRNN-V2 [18] has the best performance, however, the method is outperformed by R-ST-ConvLSTM [21] and, Conv-TT-LSTM [20] in PSNR and SSIM, respectively. Similar observations can be made for the Moving-MNIST task. It can be argued that starting from 2018, all methods are quite competitive with one another, and it is not actually possible to indicate a single technique that performs the best on the video prediction task across all

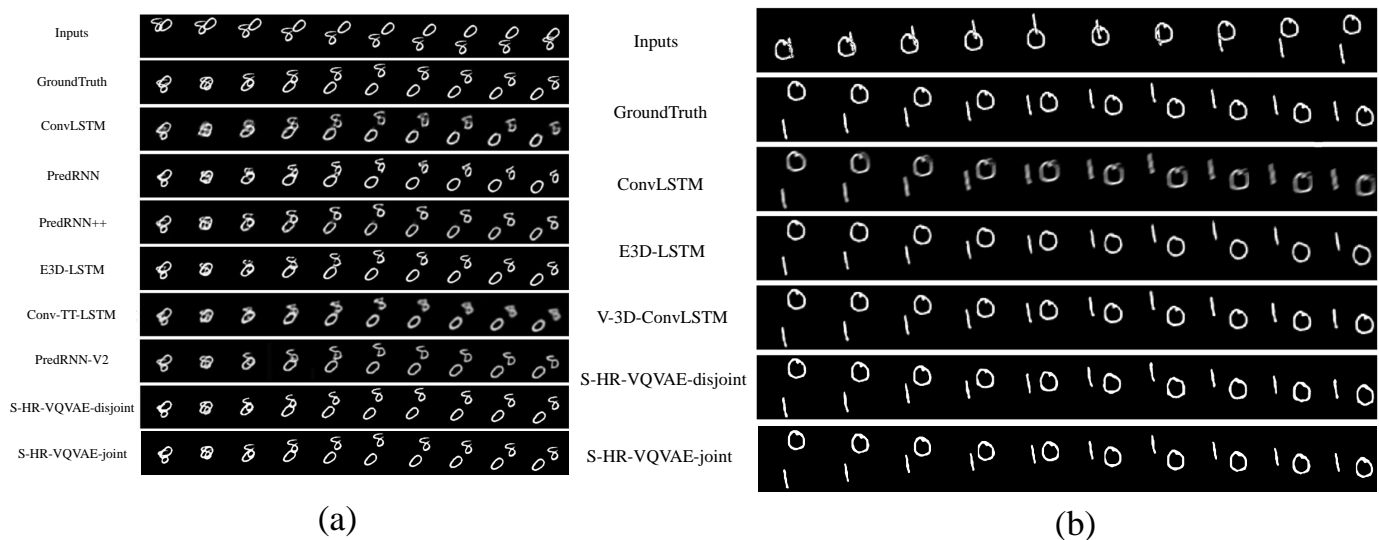


Fig. 2: Comparison of S-HR-VQVAE with state-of-the-art methods on Moving-MNIST dataset over two sequences (a and b) that are commonly reported in the literature. It should be noted that 10 frames (*Inputs* in the figures) are given as input to the models and the next 10 frames (*GroundTruth* in the figures) are the targets for the models' predictions.

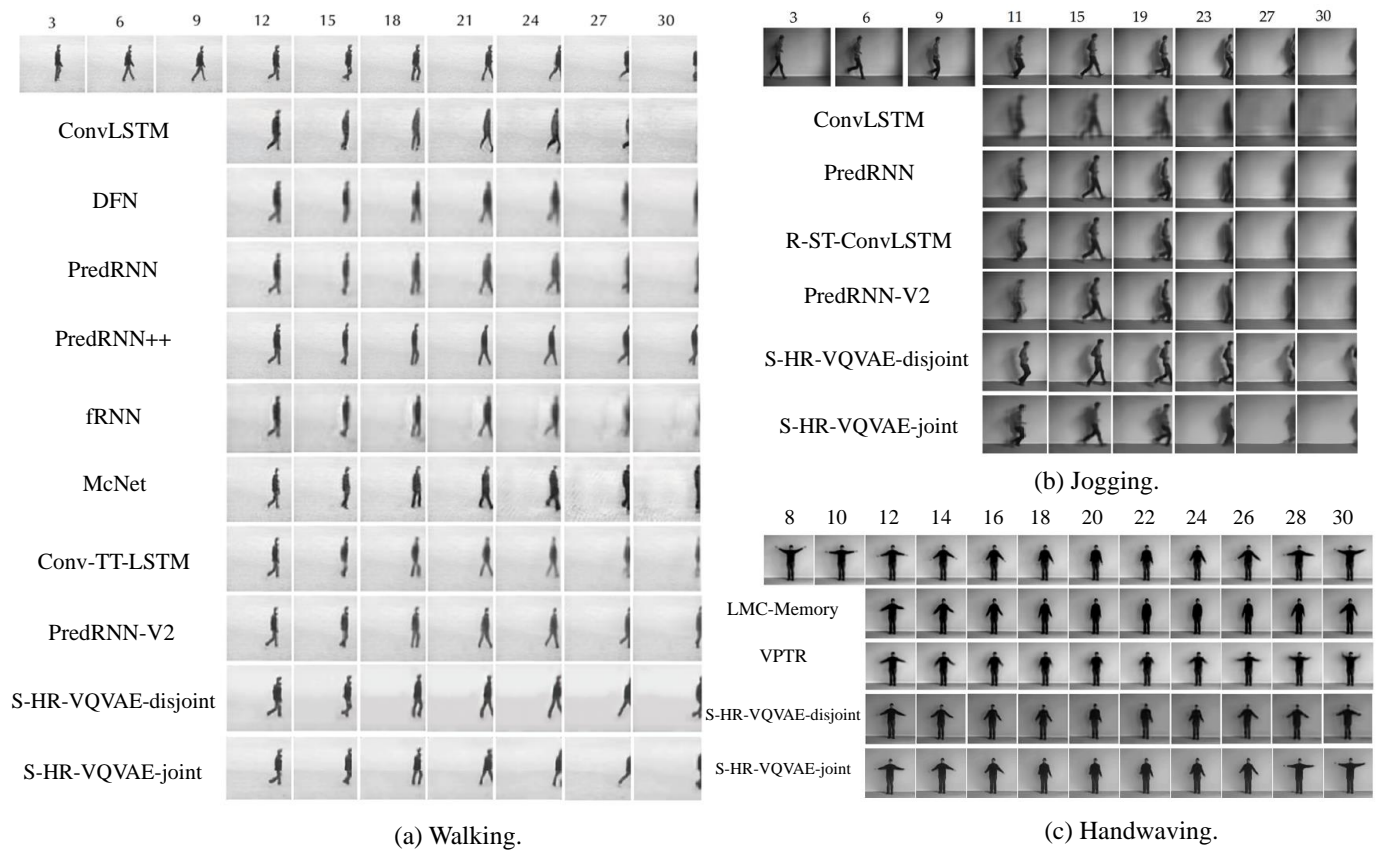


Fig. 3: Comparison of S-HR-VQVAE with state-of-the-art-methods on KTH Human Moving Action dataset over three sequences (a, b and c) that are commonly reported in the literature. It should be noted that 10 frames (1-10 in the figures) are given as input and the next 20 frames (11-30 in the figures) are predicted.

TABLE 2: Results on KTH Human Action dataset and Moving-MNIST datasets. S-HR-VQVAE with 3 layers was used with disjoint and joint training.

| Method | KTH Human Action (10 \rightarrow 20) | | | Moving-MNIST (10 \rightarrow 10) | | | |
|----------------------------|--|-----------------|--------------------|------------------------------------|-----------------|------------------|----------------------|
| | PSNR \uparrow | SSIM \uparrow | LPIPS \downarrow | PSNR \uparrow | SSIM \uparrow | MSE \downarrow | #Params \downarrow |
| ConvLSTM (2015) [15] | 23.01 | 0.704 | 0.156 | 28.38 | 0.713 | 103.3 | 16.60M |
| DFN (2016) [37] | 27.26 | 0.794 | \times | \times | 0.726 | 89.0 | \times |
| CDNA (2016) [38] | 23.75 | 0.752 | \times | \times | 0.728 | 97.4 | \times |
| DrNet(2017) [12] | 25.56 | 0.764 | \times | 14.79 | 0.650 | \times | 23.30M |
| PredRNN (2017) [16] | 27.55 | 0.839 | 0.167 | \times | 0.869 | 56.8 | 23.85M |
| McNet (2018) [13] | 25.95 | 0.804 | \times | 12.53 | 0.421 | 268.7 | 3.50M |
| MsNet (2018) [14] | 27.08 | 0.876 | \times | \times | \times | \times | 3.20M |
| fRNN (2018) [26] | 26.12 | 0.771 | \times | \times | 0.819 | 69.7 | \times |
| PredRNN++ (2018) [17] | 28.62 | 0.888 | 0.229 | \times | 0.885 | 47.9 | 15.40M |
| E3D-LSTM (2019) [19] | 27.92 | 0.893 | \times | \times | 0.910 | 44.2 | 41.94M |
| Conv-TT-LSTM (2020) [20] | 28.36 | 0.907 | 0.133 | \times | 0.924 | 53.0 | 2.69M |
| LMC-Memory (2021) [41] | 28.61 | 0.894 | 0.133 | \times | 0.924 | 41.5 | \times |
| V-3D-ConvLSTM (2021) [27] | 28.31 | 0.866 | \times | \times | 0.896 | 39.4 | 12.90M |
| R-ST-ConvLSTM (2022) [21] | 28.99 | 0.854 | \times | 32.52 | 0.895 | \times | \times |
| PredRNN-V2 (2023) [18] | 28.37 | 0.838 | 0.071 | \times | 0.891 | 48.4 | 23.86M |
| VPTR (2023) [28] | 26.96 | 0.879 | 0.076 | \times | 0.882 | 63.6 | 162.48M |
| S-HR-VQVAE-disjoint (ours) | 28.43 | 0.863 | 0.130 | 30.35 | 0.916 | 55.5 | 1.14M |
| S-HR-VQVAE-joint (ours) | 28.49 | 0.897 | 0.093 | 31.49 | 0.919 | 46.2 | 1.14M |

(\uparrow) means higher is better and (\downarrow) means lower is better.

metrics. In order to compare our method to the state-of-the-art, we have therefore decided to consider results across all available metrics.

We can see from Table 2 that the proposed S-HR-VQVAE outperforms on the KTH Human Action task all methods up to fRNN [26] in *all* reported metrics. For the methods proposed after fRNN [26], S-HR-VQVAE outperforms PredRNN++ [17] on two metrics out of three (SSIM and LPIPS), E3D-LSTM [19] on all metrics, Conv-TT-LSTM [20] on two metrics out of three (PSNR and LPIPS), LMC-Memory [41] on two metrics out of three (SSIM and LPIPS), V-3D-ConvLSTM [27] on all metrics, R-ST-ConvLSTM [21] on one out of two metrics (SSIM), and finally PredRNN-V2 [18] and VPTR [28] on two metrics out of three (PSNR and SSIM).

On the Moving-MNIST task, our method outperforms all state-of-the-art methods on *all* metrics up to PredRNN++ [17]. For the methods proposed after PredRNN++ [17], S-HR-VQVAE outperforms E3D-LSTM [19] on one out of two metrics (SSIM), Conv-TT-LSTM [20] on one out of two metrics (MSE), V-3D-ConvLSTM [27] on one out of two metrics (SSIM), R-ST-ConvLSTM [21] on one out of two metrics (SSIM), and finally PredRNN-V2 [18] and VPTR [28] on all metrics. For the Moving-MNIST task, LMC-Memory [41] outperforms our method on both reported metrics. However, we do not know how this method would perform on PSNR.

From this analysis, we can conclude that, although some of the state-of-the-art methods outperform our method on a single metric, our method seems to be more robust across all metrics for both of the considered tasks. For example, Conv-TT-LSTM [20] has the overall best SSIM both for KTH Human Action and Moving-MNIST, but we outperform it both on PSNR and LPIPS (KTH Human Action) and MSE (Moving-MNIST). R-ST-ConvLSTM [21] has the overall best

PSNR on KTH Human Action and Moving-MNIST, but we outperform it on SSIM (both on KTH Human Action and Moving-MNIST). V-3D-ConvLSTM [27] has the overall best MSE on Moving-MNIST, but S-HR-VQVAE outperforms it on SSIM (Moving-MNIST) and on all reported metrics for KTH Human Action. Finally, PredRNN-V2 [18] has the overall best LPIPS on KTH Human Action, but S-HR-VQVAE outperforms it on PSNR and SSIM for the KTH Human Action task and SSIM and MSE for the Moving-MNIST task.

It is worth mentioning that these results are obtained with an S-HR-VQVAE model that owns a number of parameters lower, and in some cases orders of magnitude lower, than that of all of the competing models.

Finally, from Table 2 we can also evince that the proposed joint training of HR-VQVAE and ST-PixelCNN has a positive effect on the results both for KTH Human Action and Moving-MNIST tasks. The effectiveness of our approach can be further appreciated by considering the following qualitative analyses. In fact, objective metrics might not capture all aspects of the the actual quality of the predicted sequence.

6.2 Qualitative Analysis

Figure 2 shows two samples commonly reported in the literature from the Moving-MNIST task in panels *a* and *b*, respectively. In both panels, the first row illustrates the input sequence, consisting of 10 frames. In the second row, the ground truth is shown — the actual 10 frames to be predicted. The goal is to accurately predict the ground truth given the input sequence. A visual inspection of the two panels reveals that S-HR-VQVAE accurately predicts the position of the two digits while preserving their structural information. In contrast, the state-of-the-art methods achieving the best results among those listed in Table 2, struggle to

maintain the structural integrity of the digits. Furthermore, S-HR-VQVAE provides sharper images than the state-of-the-art methods, which demonstrates its ability in addressing the blurry prediction problem. We conclude that S-HR-VQVAE is more effective at capturing and preserving details in the input frames, leading to more accurate predictions.

Figure 3 shows the prediction outcome for different state-of-the-art methods and S-HR-VQVAE on the KTH Human Action dataset for three different activities: walking (panel a), jogging (panel b), and handwaving (panel c). Consistently with the outcomes observed on the Moving-MNIST dataset, S-HR-VQVAE achieves remarkable precision in predicting the subject’s position while simultaneously maintaining the details of each frame, and avoiding blurry outputs. For example, in the hand wave activity, the hand movements are relatively fast, but S-HR-VQVAE is able to better predict the ground truth whilst avoiding blurry outputs, as shown in frames 28 and 30. For the walking task, most methods are not good at predicting the position of the body and the legs, with the exception of our method, PredRNN, PredRNN++ and PredRNN-V2 (see frames 27 and 30, for example). However, our method produces sharper images and correctly predicts the location of both legs for these frames. Finally, for the jogging task, we can see an overall better estimation of the location of the jogger, in addition to sharper images.

Finally, the proposed joint training in our method appears to improve the location prediction significantly compared to disjoint training. This can be observed in most frames in Figure 2 and 3. However, the sharpness of image reconstruction is somewhat reduced. This may explain why the quantitative results are only slightly better for joint training.

We can summarise the outcome of the qualitative analysis as follows: although the quantitative analysis is useful to understand whether a sequence prediction technique is viable or not, objective measures by themselves may not reveal the actual capability of a technique. In fact, state-of-the-art methods exhibit a varying sequence prediction quality across the two tasks, as observed in Figure 2 and 3 despite the good numerical results reported in Table 2. In contrast, S-HR-VQVAE attains a consistent performance on both tasks.

7 DISCUSSION

In this section, we analyze some properties of HR-VQVAE that confer unique characteristics to S-HR-VQVAE, and that can be used to better understand the results obtained in the previous section. Finally, we also investigate the effect on the final performance of different configurations.

7.1 Model Interpretability

To facilitate the interpretation of latent representations produced by the model, we present heatmaps over various layers of the HR-VQVAE in Figure 4. Each heatmap highlights regions of significance within the reconstructed latent representation. Specifically, general information, i.e., background, is mainly captured in the first layer; the second layer focuses on the position; whereas, the third layer is concerned with moving objects.

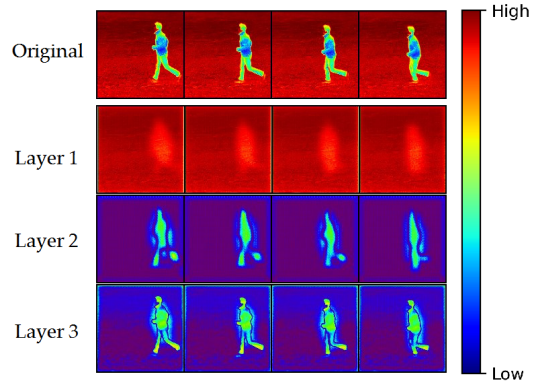


Fig. 4: Heatmap of reconstructions obtained from different layers of a 3-layer HR-VQVAE.

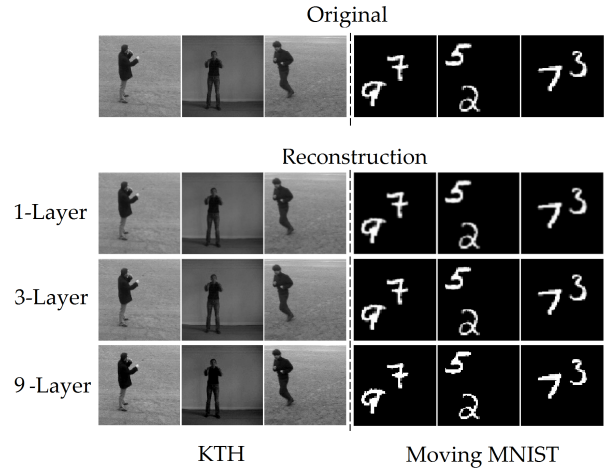


Fig. 5: Reconstructions of random frames by HR-VQVAE with different numbers of layers.

7.2 Compression Ratio and Reconstruction Quality

In Table 1, we have already reported the S-HR-VQVAE’s compression ratio achieved with different configurations. In Figure 5, we complete the analysis on the compression capability of HR-VQVAE showing reconstructed images from compressed latent codes when different numbers of layers in the quantization scheme are used. In particular, we consider three configurations having 3, 6, and 9 layers, respectively, which attain the same compression ratio. The quantized codes are approximately 42.66 and 21.33 times smaller than the original input frames for the KTH Human Action and Moving-MNIST datasets, respectively. Nonetheless, the reconstructed images shown in Figure 5 have a high quality; moreover, as the number of HR-VQVAE layers increases, the quality of the reconstructed image improves. In the configuration with 9 layers, the best image reconstruction quality is attained, as can be observed by close inspection.

High-quality reconstruction is crucial in video prediction. The ability to accurately reconstruct video frames from compressed latent representations is essential for generating realistic and visually coherent predictions. High-resolution videos, require detailed and faithful reconstruction to capture fine-grained motion and appearance dynamics. By ef-

fectively compressing high-resolution videos into a hierarchical set of multi-scale discrete latent variables, HR-VQVAE enables scalable autoregressive generative models for video prediction.

7.3 Blur Mitigation and Noise Removal

To gain more insights into the effectiveness of S-HR-VQVAE against blurriness, we artificially corrupt some video sequences by injecting Gaussian Blur (Figure 6-a), and Fragment Blur (Figure 6-b). The prediction results reported in those figures clearly demonstrate that HR-VQVAE can successfully reduce blurriness while being able to reconstruct details in the images that were lost due to the blur effect. In addition to blur mitigation, HR-VQVAE is also robust to noise, as shown in Figure 6-c, where accurate sequence prediction is attained although the input frames were artificially corrupted with additive noise at different SNR levels. HR-VQVAE robustness against blur and noise in sequence prediction is especially valuable in applications where the quality of the predicted video frames is critical, such as autonomous driving.

In addition, HR-VQVAE’s ability to remove noise at the decoding level allows for better predictions by addressing any unwanted distortions in the quantized latent representations used for prediction. This approach is highly effective, as it enables unwanted distortions to be removed at the decoder level, leading to improved prediction quality. This effect is demonstrated in Figure 7, where the combination of HR-VQVAE and ST-PixelCNN, S-HR-VQVAE, for prediction at the latent level outperforms the use of ST-PixelCNN alone for prediction at the frame level.

7.4 Impact of HR-VQVAE Configurations

Table 3 and Figure 7 show the S-HR-VQVAE performance, in terms of SSIM, PSNR, and LPIPS, under different configurations. The results indicate that an optimal performance is attained with the 3×8 S-HR-VQVAE, consisting of three layers, each with eight codebooks. It should be noted that an excessively high number of layers could result in overfitting, where the model extracts excessive detailed information that leads to fitting the model distribution to a limited set of high-variant samples, increasing the model’s bias toward certain types of information and degrading its performance. However, an insufficient number of layers could lead to underfitting, where important detailed information is overlooked, compromising the model’s ability to capture all levels of detail and leading to poor performance. Thus, we experimentally optimized the performance of S-HR-VQVAE using three layers to encode the continuous latent, allowing for a balanced extraction of detailed information that avoids bias towards any particular type of information. Through this optimization, the proposed approach achieves superior performance, highlighting the significance of considering different levels of abstraction in future video frame prediction.

8 CONCLUSION

In this study, we proposed a novel video prediction framework that combines the hierarchical vector quantization

codebooks of the previously proposed HR-VQVAE with the novel spatiotemporal PixelCNN (ST-PixelCNN). We call this method sequential HR-VQVAE (S-HR-VQVAE). We show how the proposed S-HR-VQVAE takes advantage of hierarchical frame modeling to model different levels of abstraction, enabling the system to capture both context and movements (details) in video frames with a fraction of the parameters used by competing models. We show by extensive experimental evidence on the KTH Human Action and Moving-MNIST tasks that the model is very competitive with the state-of-the-art in video prediction, outperforming the best methods at least in a subset of the available metrics (PSNR, SSIM, LPIPS and MSE). We also provide a detailed analysis of the properties of the model including an analysis of its internal representations and its behavior with respect to blurry and noisy input frames. We believe that the proposed method will be competitive for the video prediction task, both for the performance, but for the low complexity and interpretability as well.

REFERENCES

- [1] T. Lane and C. E. Brodley, “Temporal sequence learning and data reduction for anomaly detection,” *ACM Transactions on Information and System Security (TISSEC)*, vol. 2, no. 3, pp. 295–331, 1999.
- [2] Y. Seo, M. Defferrard, P. Vandergheynst, and X. Bresson, “Structured sequence modeling with graph convolutional recurrent networks,” in *International Conference on Neural Information Processing*. Springer, 2018, pp. 362–373.
- [3] V. Vukotić, S.-L. Pintea, C. Raymond, G. Gravier, and J. C. Van Gemert, “One-step time-dependent future video frame prediction with a convolutional encoder-decoder neural network,” in *International conference on image analysis and processing*. Springer, 2017, pp. 140–151.
- [4] C. Lu, M. Hirsch, and B. Schölkopf, “Flexible spatio-temporal networks for video prediction,” in *2017 IEEE Conference on Computer Vision and Pattern Recognition (CVPR)*, 2017.
- [5] R. Bellman, *Adaptive Control Processes: A Guided Tour*. Princeton University Press, 1961.
- [6] M. Adiban, K. Stefanov, S. M. Siniscalchi, and G. Salvi, “Hierarchical residual learning based vector quantized variational autoencoder for image reconstruction and generation,” in *33rd British Machine Vision Conference 2022, BMVC 2022, London, UK, November 21-24, 2022*. BMVA Press, 2022.
- [7] A. v. d. Oord, N. Kalchbrenner, O. Vinyals, L. Espeholt, A. Graves, and K. Kavukcuoglu, “Conditional image generation with PixelCNN decoders,” in *Proceedings of the 30th International Conference on Neural Information Processing Systems*, ser. NIPS’16. Red Hook, NY, USA: Curran Associates Inc., 2016, p. 4797–4805.
- [8] T. Salimans, A. Karpathy, X. Chen, and D. P. Kingma, “PixelCNN++: Improving the PixelCNN with discretized logistic mixture likelihood and other modifications,” *arXiv preprint arXiv:1701.05517*, 2017.
- [9] D. P. Kingma and M. Welling, “Stochastic gradient vb and the variational auto-encoder,” in *Second International Conference on Learning Representations, ICLR*, vol. 19, 2014.
- [10] L. Deng, “The mnist database of handwritten digit images for machine learning research [best of the web],” *IEEE Signal Processing Magazine*, vol. 29, no. 6, pp. 141–142, 2012.
- [11] C. Schuldt, I. Laptev, and B. Caputo, “Recognizing human actions: a local SVM approach,” in *Proceedings of the 17th International Conference on Pattern Recognition, 2004. ICPR 2004.*, vol. 3. IEEE, 2004, pp. 32–36.
- [12] E. Denton and V. Birodkar, “Unsupervised learning of disentangled representations from video,” in *Proceedings of the 31st International Conference on Neural Information Processing Systems*, 2017, pp. 4417–4426.
- [13] R. Villegas, J. Yang, S. Hong, X. Lin, and H. Lee, “Decomposing motion and content for natural video sequence prediction,” *arXiv preprint arXiv:1706.08033v2*, 2018.

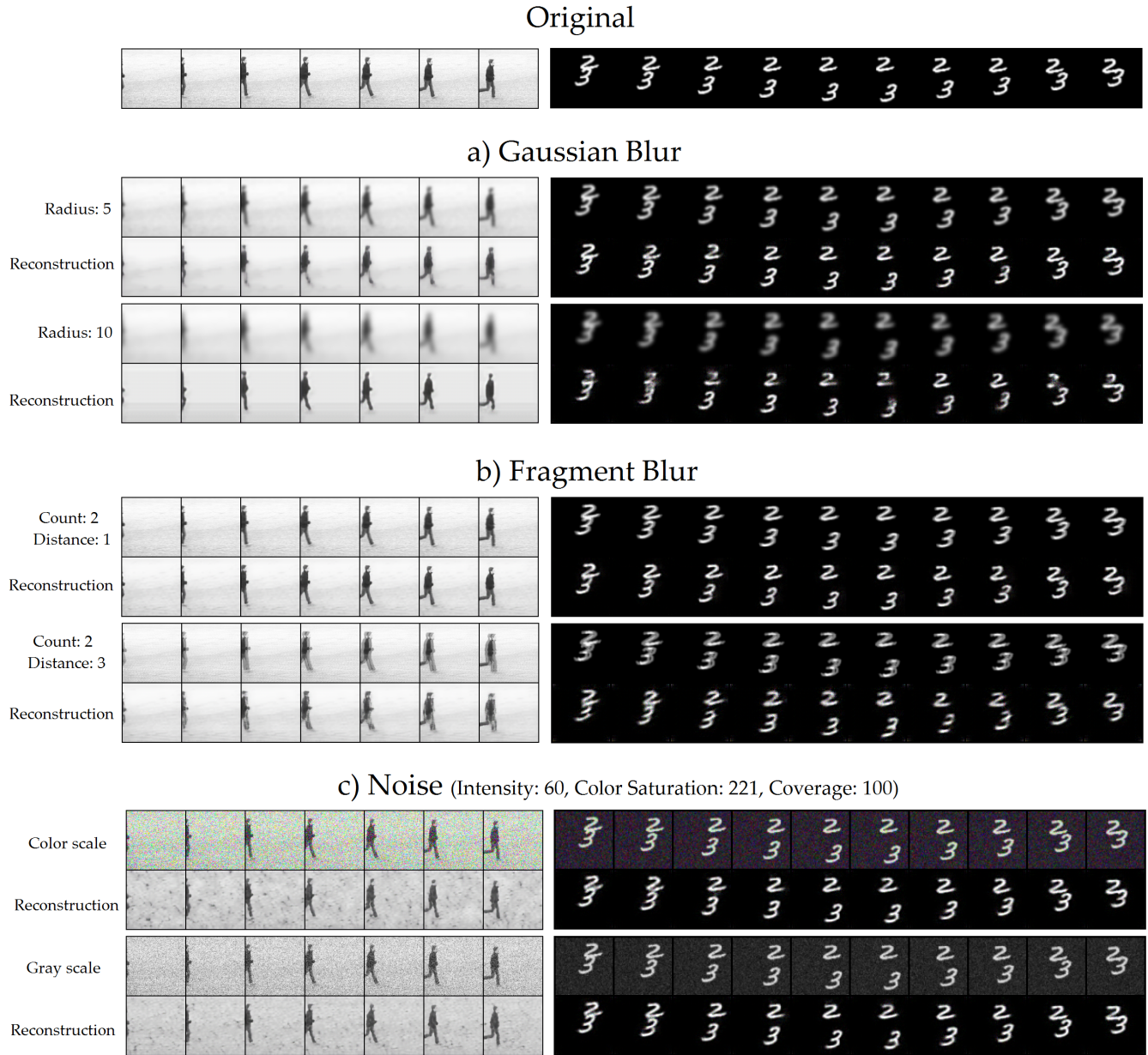


Fig. 6: Reconstructions by 3-layer HR-VQVAE. a) Gaussian Blur b) Fragment Blur c) Noise.

TABLE 3: Results on the KTH Human Action and Moving-MNIST datasets for different configurations of S-HR-VQVAE.

| Method | KTH (10 → 20) | | | Moving MNIST (10 → 10) | | |
|----------------------------|---------------|-------|--------|------------------------|-------|-------|
| | PSNR↑ | SSIM↑ | LPIPS↓ | PSNR↑ | SSIM↑ | MSE↓ |
| 1-layer S-HR-VQVAE* | 26.91 | 0.830 | 0.173 | 29.01 | 0.865 | 67.55 |
| 3-layer S-HR-VQVAE | 28.43 | 0.863 | 0.130 | 30.35 | 0.916 | 55.46 |
| 9-layer S-HR-VQVAE | 27.70 | 0.844 | 0.148 | 29.86 | 0.902 | 61.73 |
| 3-layer S-HR-VQVAE (joint) | 28.49 | 0.897 | 0.093 | 31.49 | 0.919 | 46.20 |

* Equivalent to VQVAE + ST-PixelCNN

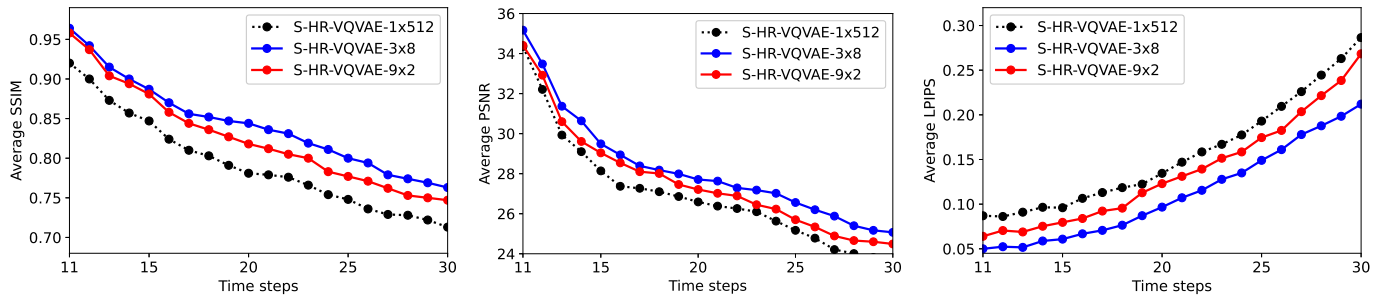


Fig. 7: Performance in terms of SSIM (left), PSNR (center), and LPIPS (right) for different configurations of S-HR-VQVAE.

- [14] J. Lee, J. Lee, S. Lee, and S. Yoon, "Mutual suppression network for video prediction using disentangled features," *arXiv preprint arXiv:1804.04810*, 2018.
- [15] X. Shi, Z. Chen, H. Wang, D.-Y. Yeung, W.-K. Wong, and W.-c. Woo, "Convolutional lstm network: A machine learning approach for precipitation nowcasting," *Advances in neural information processing systems*, vol. 28, 2015.
- [16] Y. Wang, M. Long, J. Wang, Z. Gao, and P. S. Yu, "Predrnn: Recurrent neural networks for predictive learning using spatiotemporal lstms," *Advances in neural information processing systems*, vol. 30, 2017.
- [17] Y. Wang, Z. Gao, M. Long, J. Wang, and S. Y. Philip, "Predrnn++: Towards a resolution of the deep-in-time dilemma in spatiotemporal predictive learning," in *International Conference on Machine Learning*. PMLR, 2018, pp. 5123–5132.
- [18] Y. Wang, H. Wu, J. Zhang, Z. Gao, J. Wang, S. Y. Philip, and M. Long, "Predrnn: A recurrent neural network for spatiotemporal predictive learning," *IEEE Transactions on Pattern Analysis and Machine Intelligence*, vol. 45, no. 2, pp. 2208–2225, 2023.
- [19] Y. Wang, L. Jiang, M.-H. Yang, L.-J. Li, M. Long, and L. Fei-Fei, "Eidetic 3d lstm: A model for video prediction and beyond," in *International conference on learning representations*, 2019.
- [20] J. Su, W. Byeon, J. Kossaiji, F. Huang, J. Kautz, and A. Anandkumar, "Convolutional tensor-train lstm for spatio-temporal learning," *Advances in Neural Information Processing Systems*, vol. 33, pp. 13714–13726, 2020.
- [21] W. Saideni, D. Helbert, F. Courreges, and J. P. Cances, "A novel video prediction algorithm based on robust spatiotemporal convolutional long short-term memory (robust-st-convlstm)," in *Proceedings of Seventh International Congress on Information and Communication Technology: ICICT 2022, London, Volume 2*. Springer, 2022, pp. 193–204.
- [22] M. Ranzato, A. Szlam, J. Bruna, M. Mathieu, R. Collobert, and S. Chopra, "Video (language) modeling: a baseline for generative models of natural videos," *arXiv preprint arXiv:1412.6604*, 2014.
- [23] C. Xu, P. Zhao, Y. Liu, J. Xu, V. S. S. Sheng, Z. Cui, X. Zhou, and H. Xiong, "Recurrent convolutional neural network for sequential recommendation," in *The world wide web conference*, 2019, pp. 3398–3404.
- [24] J.-T. Hsieh, B. Liu, D.-A. Huang, L. F. Fei-Fei, and J. C. Niebles, "Learning to decompose and disentangle representations for video prediction," in *Advances in Neural Information Processing Systems*, 2018, pp. 517–526.
- [25] T. Xue, J. Wu, K. Bouman, and B. Freeman, "Visual dynamics: Probabilistic future frame synthesis via cross convolutional networks," in *Advances in neural information processing systems*, 2016, pp. 91–99.
- [26] M. Oliu, J. Selva, and S. Escalera, "Folded recurrent neural networks for future video prediction," in *Proceedings of the European Conference on Computer Vision (ECCV)*, 2018, pp. 716–731.
- [27] H. Razali and B. Fernando, "A log-likelihood regularized kl divergence for video prediction with a 3d convolutional variational recurrent network," in *Proceedings of the IEEE/CVF Winter Conference on Applications of Computer Vision*, 2021, pp. 209–217.
- [28] X. Ye and G.-A. Bilodeau, "Video prediction by efficient transformers," *Image and Vision Computing*, vol. 130, p. 104612, 2023.
- [29] L. Castrejon, N. Ballas, and A. Courville, "Improved conditional vrns for video prediction," in *Proceedings of the IEEE International Conference on Computer Vision*, 2019, pp. 7608–7617.
- [30] A. B. L. Larsen, S. K. Sønderby, H. Larochelle, and O. Winther, "Autoencoding beyond pixels using a learned similarity metric," *arXiv preprint arXiv:1512.09300*, 2015.
- [31] A. X. Lee, R. Zhang, F. Ebert, P. Abbeel, C. Finn, and S. Levine, "Stochastic adversarial video prediction," *arXiv preprint arXiv:1804.01523*, 2018.
- [32] M. Mathieu, C. Couprie, and Y. LeCun, "Deep multi-scale video prediction beyond mean square error," *arXiv preprint arXiv:1511.05440*, 2015.
- [33] M. Babaeizadeh, C. Finn, D. Erhan, R. H. Campbell, and S. Levine, "Stochastic variational video prediction," *arXiv preprint arXiv:1710.11252*, 2017.
- [34] E. Denton and R. Fergus, "Stochastic video generation with a learned prior," *arXiv preprint arXiv:1802.07687*, 2018.
- [35] O. Barnich and M. Van Droogenbroeck, "Vibe: a powerful random technique to estimate the background in video sequences," in *2009 IEEE international conference on acoustics, speech and signal processing*. IEEE, 2009, pp. 945–948.
- [36] M. J. Primus, K. Schoeffmann, and L. Böszörményi, "Segmentation of recorded endoscopic videos by detecting significant motion changes," in *2013 11th International Workshop on Content-Based Multimedia Indexing (CBMI)*. IEEE, 2013, pp. 223–228.
- [37] X. Jia, B. De Brabandere, T. Tuytelaars, and L. V. Gool, "Dynamic filter networks," *Advances in neural information processing systems*, vol. 29, 2016.
- [38] C. Finn, I. Goodfellow, and S. Levine, "Unsupervised learning for physical interaction through video prediction," in *Advances in neural information processing systems*, 2016, pp. 64–72.
- [39] Z. Liu, R. A. Yeh, X. Tang, Y. Liu, and A. Agarwala, "Video frame synthesis using deep voxel flow," in *Proceedings of the IEEE International Conference on Computer Vision*, 2017, pp. 4463–4471.
- [40] M. Jaderberg, K. Simonyan, A. Zisserman et al., "Spatial transformer networks," in *Advances in neural information processing systems*, 2015, pp. 2017–2025.
- [41] S. Lee, H. G. Kim, D. H. Choi, H.-I. Kim, and Y. M. Ro, "Video prediction recalling long-term motion context via memory alignment learning," in *Proceedings of the IEEE/CVF Conference on Computer Vision and Pattern Recognition*, 2021, pp. 3054–3063.
- [42] A. Razavi, A. van den Oord, and O. Vinyals, "Generating diverse high-fidelity images with vq-vae-2," in *Advances in Neural Information Processing Systems*, 2019, pp. 14837–14847.
- [43] D. P. Kingma and J. Ba, "Adam: A method for stochastic optimization," *arXiv preprint arXiv:1412.6980*, 2014.
- [44] S. Winkler and P. Mohandas, "The evolution of video quality measurement: From psnr to hybrid metrics," *IEEE transactions on Broadcasting*, vol. 54, no. 3, pp. 660–668, 2008.
- [45] V. Sitzmann, M. Zollhöfer, and G. Wetzstein, "Scene representation networks: Continuous 3d-structure-aware neural scene representations," *Advances in Neural Information Processing Systems*, vol. 32, 2019.
- [46] R. Zhang, P. Isola, A. A. Efros, E. Shechtman, and O. Wang, "The unreasonable effectiveness of deep features as a perceptual metric," in *Proceedings of the IEEE conference on computer vision and pattern recognition*, 2018, pp. 586–595.
- [47] S. Mrak et al., "Reliability of objective picture quality measures," *Journal of Electrical Engineering*, vol. 55, no. 1-2, pp. 3–10, 2004.
- [48] Z. Wang, A. C. Bovik, H. R. Sheikh, and E. P. Simoncelli, "Image quality assessment: from error visibility to structural similarity," *IEEE transactions on image processing*, vol. 13, no. 4, pp. 600–612, 2004.
- [49] X. Fei, L. Xiao, Y. Sun, and Z. Wei, "Perceptual image quality assessment based on structural similarity and visual masking,"

Signal Processing: Image Communication, vol. 27, no. 7, pp. 772–783, 2012.



Mohammad Adiban is a PhD candidate in Machine Learning at the Norwegian University of Science and Technology (NTNU). He holds a Bachelor's degree in Computer Engineering and a Master's degree in Artificial Intelligence from the Sharif University of Technology, awarded in 2017. In 2022, he conducted research as a visiting scholar at Monash University in Australia. Additionally, Mohammad is a co-founder of the company Connect Me. His research focuses on statistical machine learning, signal processing, computer vision, speech processing, biomedical applications, and cyber security.



Kalin Stefanov is an ARC DECRA Fellow at the Faculty of Information Technology, Monash University, Melbourne, Australia. He received the MSc degree in Artificial Intelligence from the University of Amsterdam, Amsterdam, Netherlands and a PhD degree in Computer Science from KTH Royal Institute of Technology, Stockholm, Sweden. Prior to his current role, he was a Research Associate and Postdoctoral Research Scholar at University of Southern California, Los Angeles, USA. His main research interests are machine learning, computer vision, and affective computing.



Sabato Marco Siniscalchi (Senior Member, IEEE) is a Professor with the University of Enna, Enna, Italy, an Adjunct Professor with the Norwegian University of Science and Technology's (NTNU), and an Affiliate Faculty with the Georgia Institute of Technology. He received his doctorate degree in computer engineering from the University of Palermo, Palermo, Italy, in 2006. In 2006, he was a Postdoctoral Fellow with Ga Tech. From 2007 to 2010, he joined NTNU, Norway, as a Research Scientist. From 2010 to 2015, he was an Assistant Professor, first, and an Associate Professor, after, at the Kore University. From 2017 to 2018, he was a Senior Speech Researcher with Siri Speech Group, Apple Inc., Cupertino CA, USA. He acted as an Associate Editor of the IEEE/ACM Transactions on Audio, Speech and Language Processing, from 2015 to 2019. Prof. Siniscalchi was an Elected Member of the IEEE SLT Committee from 2019 to 2022.



Giampiero Salvi is Professor at the Department of Electronic Systems at the Norwegian University of Science and Technology (NTNU), Trondheim, Norway, and Associate Professor at KTH Royal Institute of Technology, Department of Electrical Engineering and Computer Science, Stockholm, Sweden. Prof. Salvi received the MSc degree in Electronic Engineering from Università la Sapienza, Rome, Italy and the PhD degree in Computer Science from KTH. He was a post-doctoral fellow at the Institute of Systems and Robotics, Lisbon, Portugal. He was a co-founder of the company SynFace AB, active between 2006 and 2016. His main interests are machine learning, speech technology, and cognitive systems.